J Fluoresc (2014) 24:727–733
DOI 10.1007/s10895-013-1345-0

ORIGINAL PAPER

Elucidation of Selectivity for Uranyl Ions with an ICT Organosilane-Modified Fluorescent Receptor

Fehmi Karagöz · Orhan Güney

Received: 6 August 2013 / Accepted: 27 December 2013 / Published online: 10 January 2014

Abstract A fluorescent receptor, isocyanatopropyl trimethoxysilane grafted 9-amino acridine (*AcI*), was synthesized and characterized by elemental analysis, FTIR and NMR spectroscopy. Photophysical properties and pH-dependent fluorescence behavior of *AcI* were investigated and its complex stoichiometry with uranyl ion was elucidated. Change in fluorescence emission of *AcI* with pH of the solution was observed and pKa value was determined by using integrated emission intensity versus pH. It was found that *AcI* exhibited fluorescence enhancement, which can be attributed to an internal charge transfer (ICT) mechanism, upon titration with uranyl ions in mixture of ethanol-buffer solution while the fluorescence emission of *AcI* was not affected by addition of other divalent transition metal ions except mercury (II) ions. On the other hand, the both fluorescence and UV-vis titration measurements revealed unique selectivity for uranyl ions over the interfering mercury (II) ions. The spectrofluorometric titration clarified that uranyl interacted with *AcI* to form AcI_2 $(UO_2^{2+})_3$ (2:3) complex structure with an apparent association constant of $K=7.41\times10^6$ $M^{-2/3}$. The interference effect of some cations on fluorescence enhancement exhibited by complex was also tested.

Keywords Fluorescent receptor · ICT · Uranyl ion · Complex stoichiometry

Introduction

Uranium is a soil and water contaminant at during the processing of uranium mining and nuclear fuel production [1–3]. Under environmental conditions, uranium typically occurs in the hexavalent form as the mobile aqueous uranyl ion (UO_2^{2+}), which can be found in soils around nuclear waste sites and processing facilities. Uranyl ion is transported through the most soil matrices and the rate of uranyl migration depends on a variety of parameters including soil porosity and composition, water content and temperature [4,5]. Uranium and its compounds are highly toxic and may lead to kidney failure and death. The inhalation of uranium compounds results in deposition of uranium in lungs, which reach kidneys through the blood stream [6].

There has been a growing interest in low-cost rapid techniques for measuring heavy metal ions and polluting wastes in environmental water [7–9]. The determination of uranium is crucial in a number of nuclear related applications, such as environmental monitoring, fuel preparation and reprocessing [10–12]. The sensitive and selective photometric reagents and improving existing procedures have been dedicated to develop simple and accessible procedures for the analysis of uranyl ion [13–17]. Spectrophotometric methods are still indispensable because of their simplicity, rapidity and wide applications [18–22]. Spectrophotometric analysis will diminish the demand to apply techniques that require expensive equipment with higher operation costs such as inductively coupled plasma–mass spectrometry [23], alpha spectrometry [24], neutron activation analysis [25], X-ray fluorescence [26], gamma spectrometry [27], laser fluorimetry [28]. Although the above methods have good sensitivity, they all have some drawbacks, some of which require extensive chemical manipulation and well-controlled experimental conditions, and some may suffer from many types of interferences.

A fluorescent sensor based on intramolecular charge transfer (ICT) mechanism does not have any spacer [29,30]. If a receptor, as an electron donor within the fluorophore, is directly connected with a conjugation system and forms a new conjugation system with π-

F. Karagöz · O. Güney (✉)
Department of Chemistry, Istanbul Technical University,
34469 Istanbul, Turkey
e-mail: oguney@itu.edu.tr

electron, resulting in electron rich and electron poor terminals, then ICT from the electron donor to receptor would be enhanced upon excitation by light [31,32] In this study, we present *AcI* as fluorophore which has a strong "push-pull" π-electron system, with the pyridine nitrogen atoms as the electron donor, and ureido group, as the electron acceptor and *AcI* undergoes an ICT from the donor to the acceptor [33].

Experimental

Chemicals

9-amino acridine hydrochloride monohydrate was purchased from Aldrich and 3-isocyanatopropyl trimethoxysilane (*ICPTS*) was provided by Alfa Aesar (Lancaster, UK). Uranyl nitrate hexahydrate, $UO_2(NO_3)_2.6H_2O$, the other metal salts and chemicals were obtained from Merck (Darmstad, Germany). The organic solvents were of HPLC grade and all chemicals were used as received.

Apparatus

All pH measurements were made with a VWR pH-Meter 730P. Attenuated Total Reflectance-Infrared (ATR-FTIR) spectra were recorded on a Perkin Elmer Spectrum v5.0.1 FTIR spectrometer. ^{1}H NMR spectra were recorded on a Agilent VNMRS 500 MHz spectrometer. UV-visible spectra of samples were recorded with a VWR UV-1600 PC Spectrophotometer controlled by means of a PC. A Varian Cary-Eclipse Luminescence Spectrometer was used for recording spectra and making fluorescence measurements. It was controlled by a microprocessor fitted with a Cary-Eclipse software package for data collection and treatment. The following instrumental parameters were employed: excitation and emission slit widths were both set at 5 nm and photomultiplier voltage was 720 V.

The Synthesis of *AcI*

9-aminoacridine (*Ac*) was precipitated in neutral aqueous media by the reaction of 9-aminoacridine hydrochloride with KOH dissolved in water and was collected on a funnel by filtration. The precipitate was washed with water and dried in vacuum at room temperature. *AcI* was synthesized according to a procedure [34], with some modifications in purification method (Fig. 1). About 0.388 g of *Ac* was dissolved in 10 mL of THF dehydrated by molecular sieve, and then 2 mmol of *ICPTS* in 1 mL of dry THF was added drop wise into this mixture at room temperature. The mixture was stirred for 1 h at room temperature and then for 24 h

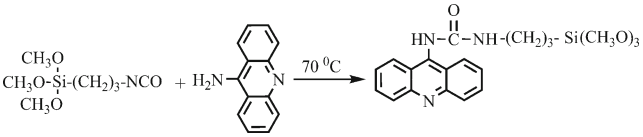

Fig. 1 Scheme of the synthesis process of *AcI*

at 70 °C under N_2. After evaporation of THF, the residue was purified by flash column chromatography (silica gel, $CHCl_3/CH_3OH$=20/1, v/v) to provide *AcI* as (58 mg, 76.2 %) yellow colored compound. ^{1}H NMR (500 MHz, DMSO-d6, 25 °C) : δ=9.13 (br, 1H, –NH–), 8.25–7.54 (4xdd, 8H, Ar–H), 6.67 (br, 1H, –NH–), 3.75 (m, 9H, $-SiO(CH_3)_3$), 3.26 (m, 2H, $-NHCH_2-$), 1.57 (m, 2H, $-CH_2CH_2-$), 0.60 (t, 2H, $-CH_2Si-$).

Results and Discussion

The structure of *AcI* was confirmed by comparing the FT-IR spectra of both *ICPTS* and *AcI* (Fig. 2) which show the functional groups before and after coupling. The cyanate group, which contributes a strong vibration band at 2266 cm^{-1}, is clearly seen in the *ICPTS* spectrum and completely disappears in the *AcI* spectrum. The peaks at 3316 cm^{-1} and 1699 cm^{-1} reveal urea structure formed in *AcI* belonging to N-H symetrical streching and C = O streching, respectively. In addition, the presence of specifically the stretching vibration of Si–O–R at 1076 cm^{-1} shows that the alkoxysilane is unhydrolyzed.

The fluorescence quantum yield of *AcI* was determined by using quinine sulfate as the standard (Φ_{ref}=0.546 in 0.1 N H_2SO_4) [35]. The experiments were done using optically matching solutions. Emission spectra were recorded upon excitation at wavelength of 365 nm and it is assumed that the sample and the reference are excited at the same wavelength so that it is not necessary to correct for the different excitation intensities of different wavelengths. Fluorescence

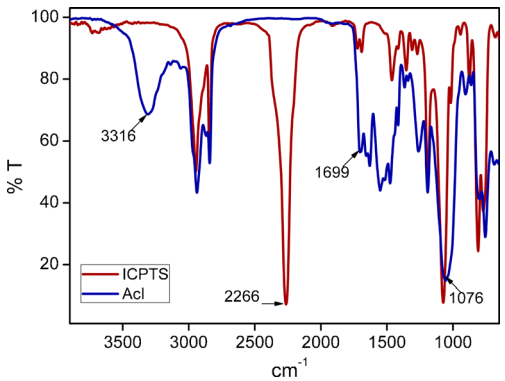

Fig. 2 The FTIR spectra of *ICPTS* and *AcI*

quantum yield of *AcI* (Φ_F) was determined according to the following equation;

$$\Phi_s = \Phi_{ref}\left(\frac{F_s}{F_{ref}}\right)\left(\frac{A_{ref}}{A_s}\right)\left(\frac{n_s^2}{n_{ref}^2}\right) \quad (1)$$

where F_s and F_{ref} are integrated area under the fluorescence emission spectra measured of sample and standard, respectively; A_s and A_{ref} are absorbances at the same excitation wavelengths of sample and standard, respectively; n_s and n_{ref} are refractive indexes of solvent used for sample and standard, and Φ_{ref} is quantum yield of standard. Fluorescence quantum yield of *AcI* was determined in ethanol as Φ_F=0.067. When compared to quantum yield of 9-amino acridine (Φ_F 0.98), the low quantum yield is due to the grafting reaction of acridine with the silicon coupling agent which may interfere with the extensive conjugation caused by alternative double bonds and enlarge the energy difference among levels of electron transition [36].

Influence of pH on the Sensor Performance

The influence of pH on fluorescent property of *AcI* and complex structure was studied in the range of 3.0–10.0 and the change in the emission intensity of *AcI* in ethanol solution at different pH values was obtained (Fig. 3). As seen from Fig. 3, the formation of complex is relatively constant in the pH range of 4.0–7.0. At pH values lower than 4.0, however, the percent recoveries decreased, which is due to the competition of H^+ ions with UO_2^{2+} ions for reaction with the *AcI*. Because pH value of higher than 4.0 would suffice to convert the more basic pyridino nitrogen into the corresponding ammonium ions. Thus the "switch on" state of fluorescence takes place in the presence of proton because the electron pair of the pyridino nitrogen is shared by proton, which inhibits ICT from urea nitrogen to excited acridine unit and induces the fluorescence increase [37]. It can be clearly seen in Fig. 3, at pH values higher than 7.0, the percent recoveries also decreased because of electrostatic interaction between OH^- ions and uranyl ions.

The plot of fluorescence intensity of *AcI* against pH displays a sigmoid profile in Fig. 3. Analysis according to the following equation gives acidic dissociation constant of *AcI* [38].

$$pK_a = pH + \log\left(\frac{\int F - \int F_{\min}}{\int F_{\max} - \int F}\right) \quad (2)$$

Where F_{max} and F_{min} refer to the maximum and minimum values of fluorescence emission during the variation of pH values and pK_a is the corresponding acidic dissociation constant. The pK_a value of *AcI* was determined by using the integrated emission intensity for each pH values and has been calculated as pK_a=3.12±0.06.

The fluorescence spectrum of *AcI* alone exhibits emission maxima at 430 nm and 453 nm in solution (Fig. 4). Upon addition of uranyl ions to the solution, the emission intensity of *AcI* at 430 nm decreases but intensity at 453 nm increases and red-shifts to 460 nm, and at the same time, new emission maximum at 485 nm appears. Fluorescence enhancement in spectra of *AcI* for different concentrations of uranyl ions indicates disruption of quenching path way because of complex formation (Fig. 4, inset). Without uranyl ions, *AcI* has low-fluorescent as there is no ICT from the tertiary amine group in pyridino moiety to the ureido moiety. However, upon coordination of uranyl ion with the urethane moiety and tertiary amine, ICT becomes operative responsible for the emission enhancement at 460 nm along with the appearance of a red shift in fluorescence [39]. Same fluorescence enhancement in spectra of *AcI* was observed upon addition of different concentrations of Hg^{2+} ions (Data were shown in interference part).

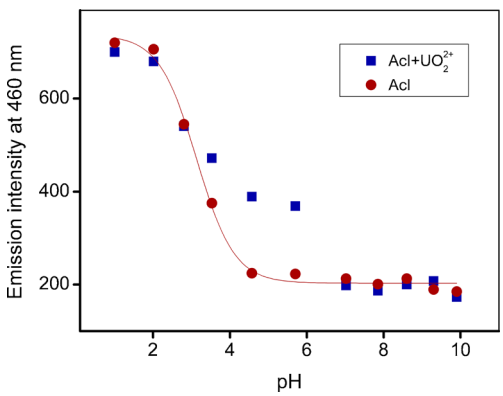

Fig. 3 The variation of fluorescence area of *AcI* (10 μM) in the absence (**a**) and in the presence of uranyl ion over a pH range from 3.0 to 10.0 at room temperature

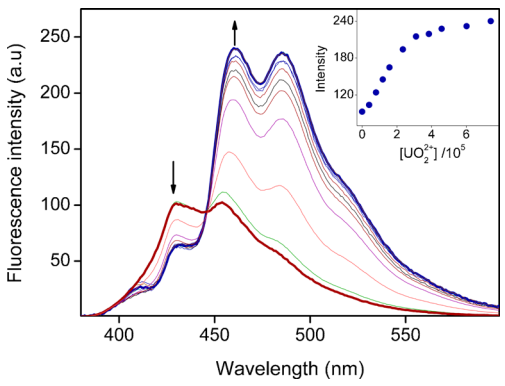

Fig. 4 Emission spectra of *AcI* (10 μM) upon addition of UO_2^{2+} ions in ethanol-acetate buffer solution (9:1, v/v) at pH 4.5. Inset: Change in emission intensity at 460 nm depending on concentrations of UO_2^{2+} ions. λ_{ex}=365 nm

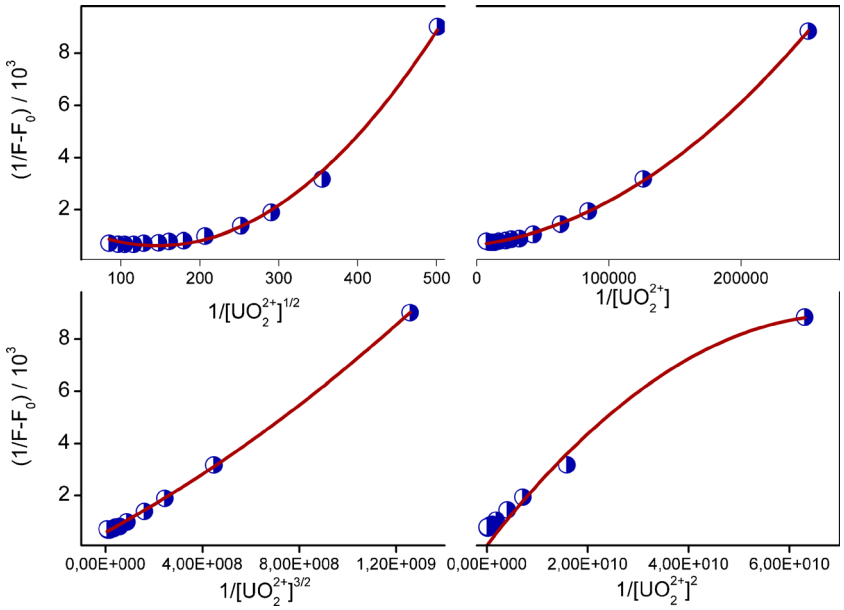

Fig. 5 Quadruple-reciprocal plots of complex structures. Straight line on the left below displays the complex of $(AcI)_2(UO_2^{2+})_3$

Complex Stoichiometry and Association Constant

When *AcI* forms coordination complex with uranyl ion, the following expression can be written;

$$nAcI + mUO_2^{2+} \rightleftharpoons (AcI)_n\left(UO_2^{2+}\right)_m \quad (3)$$

The formation constant of the coordination complex, K is given by:

$$K = \frac{\left[AcI_n\left(UO_2^{2+}\right)_m\right]}{[AcI]^n\left[UO_2^{2+}\right]^m} \quad (4)$$

Where $[AcI]$, $[UO_2^{2+}]$ and $[AcI_n(UO_2^{2+})_m]$ are equilibrium concentrations. The direct relation between the observed fluorescence intensity enhancement (F-F_0) and the using expression to that UO_2^{2+} concentration is given by: [40]

$$F - F_0 = \frac{(F_\infty - F_0)K\left[UO_2^{2+}\right]}{\left(1 + K\left[UO_2^{2+}\right]\right)} \quad (5)$$

Where F_0 denotes the fluorescence intensity of *AcI* in the absence of UO_2^{2+} ions and F_∞ denotes the fluorescence intensity when all of the *AcI* are essentially complexed with UO_2^{2+} ions. F is the observed fluorescence at each UO_2^{2+} ion concentration tested. By typical double-reciprocal plots (method of Benesi–Hilderbrand) obtained by fitting a quadruple-reciprocal plots $(1/F-F_0)$ versus $(1/[UO_2^{2+}]^{m/n})$ as can be seen in Fig. 5.

$$\frac{1}{(F-F_0)} = \frac{1}{(F_\infty - F_0)K\left[UO_2^{2+}\right]^{m/n}} + \frac{1}{(F_\infty - F_0)} \quad (6)$$

By changing m value, m=1, 2, 3, 4 and keeping n constant (n=2), when the plots of$(1/F-F_0)$ versus $1/[UO_2^{2+}]^{m/n}$ are drawn, the linearity for m=3 shows the stoichiometry of the complex is 3:2 and the association constant was calculated as to be $K=7.41\times10^6$ $M^{-2/3}$.

Interference of Foreign Metal Ions

The interference effect of diverse transition–metal ions on the fluorescence emission of *AcI* was investigated upon addition of increasing amounts of metal ions and the fluorescence spectra were recorded in ethanol-acetate buffer solution at pH 4.0. The fluorescence response of *AcI* to different metal ions was displayed in Fig. 6. As seen from Fig. 6, fluorescence emission of *AcI* quenched by adding Fe^{2+}, Cd^{2+},Ni^{2+}, Cu^{2+}, Ag^{+}, and Pb^{2+}. In general, some open-shell transition and post-transition cations often quench the fluorescence of fluorophores through the electron or energy transfer between these metal cations and fluorophores, resulting in fluorescence decrease [41], whereas, the fluorescence enhancement of *AcI* was observed when UO_2^{2+} and Hg^{2+} are added. The

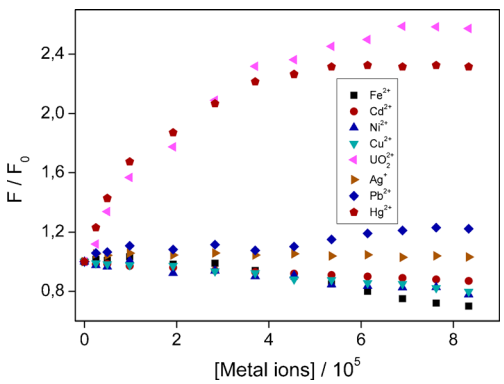

Fig. 6 The effect of metal ions on fluorescence spectrum of *AcI* in ethanol-acetate buffer (9:1, v/v) at pH 4.5. $[AcI]=1.0\times10^{-5}$ mol L^{-1}

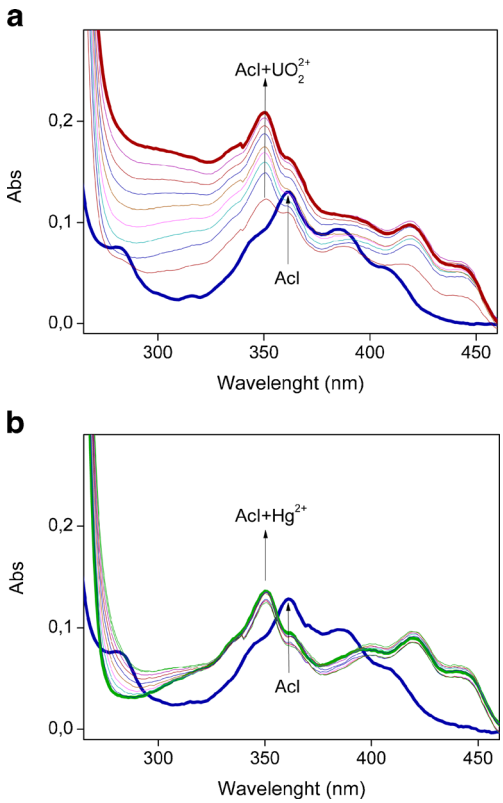

Fig. 7 Change in UV-vis absorption spectra of *AcI* (20 μM) measured in ethanol-acetate buffer upon addition of UO_2^{2+} ions (**a**) and Hg^{2+} ions (**b**)

fluorescence enhancement of *AcI* might be due to the interception of ICT process when binding to these cations [42].

UV-vis Study of Complexation

To explore the absorption properties of *AcI* as a sensing material for the uranyl ion, in preliminary experiments among various metal ions tested, it was found that the addition of proper amounts of uranyl to the solution of *AcI* results in a change in the UV-vis spectra and hypsochromic shift was observed (Fig. 7a). Maximum of wavelength shifts to 350 nm from 360 nm and intensity of absorbance increases

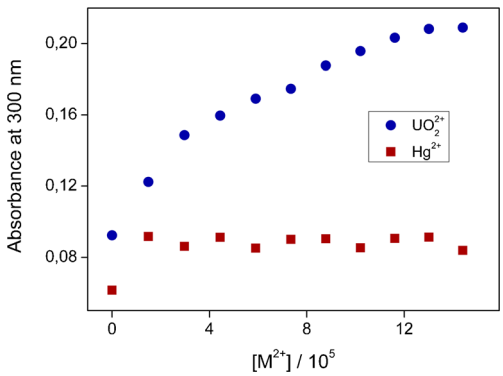

Fig. 8 Change in absorbance of *AcI* (20 μM) depending on uranyl and mercury (II) ions concentrations

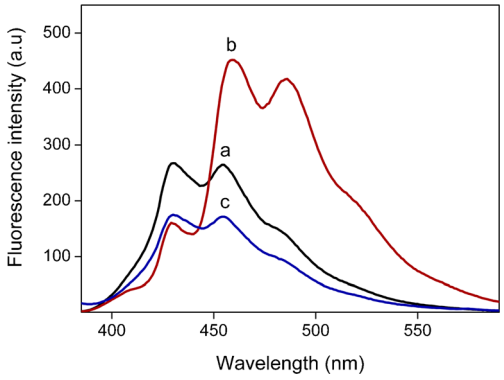

Fig. 9 Fluorescence intensity of *AcI* (10 μM) in ethanol-acetate buffer (9:1, v/v) solution at pH 4.5 (**a**) and in the presence of 50 μM UO_2^{2+} ions (**b**) and upon addition of 50 mM sodium dithionite (**c**)

upon addition of uranyl ions and also new peaks with maximum at 420 and 445 nm appeared. This is due to the reduction in π-electron conjugation in acridine ring causing to enlargement in energy level of electron transition when *AcI* bound to uranyl ion [43].

Although it was also observed a blue shift in major π–π* electronic transitions of *AcI* in the presence of Hg^{2+} but there was no increase in optical density of *AcI* at 350 nm (Fig. 7b). Compared to ultraviolet absorption spectra of *AcI* upon addition of uranyl ions with those of Hg^{2+} ions, it is clearly seen that there is a distinctive increase in the presence of uranyl ion (Fig. 8).

The Reversibility of *AcI* / UO_2^{2+} Interaction

Since the reversible chemosensor can monitor the dynamic changes in analyte concentration in the environment, the reversibility of the chemosensor is a very important aspect for some biological applications. Sodium ditionite which has strong affinity for uranyl ion was introduced into the solution containing 10 μM of *AcI* and 50 μM of UO_2^{2+} to demonstrate the reversibility of complex formation [44]. As seen from

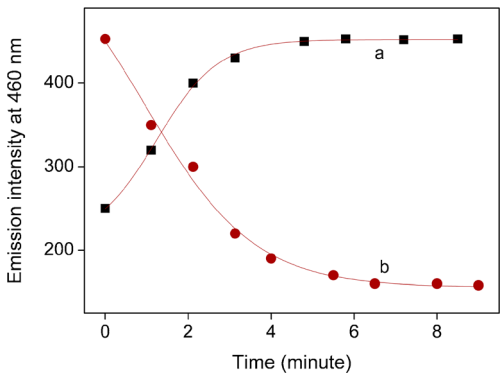

Fig. 10 Time response curves of *AcI* upon the addition of UO_2^{2+} ion (**a**) and sodium dithionite (**b**) in ethanol-buffer solution (9:1, v/v) with pH of 4.5

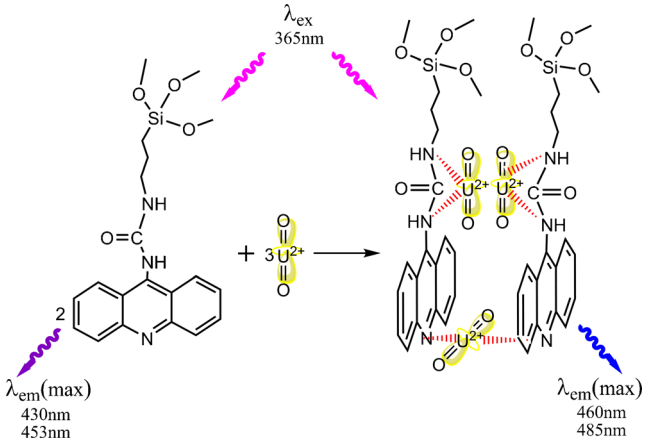

Fig. 11 The proposed binding model of *AcI* with uranyl ion

Fig. 9, fluorescence emission of *AcI* which was enhanced in the presence of UO_2^{2+} reduced and shifted to blue region because of the decomposition of complex. The reason of which fluorescence intensity was lower than that of initial value was opacity of the solution because of colloidal complex formation between uranyl ion and ditionite indicating the de-complexation of *AcI*.

The response time was obtained when *AcI* was first exposed to uranyl ion concentration of 5.0×10^{-5} mol/dm^3 and then sodium dithionite concentration of 5.0×10^{-2} mol/dm^3. Maximum enhancement in fluorescence intensity of *AcI* was observed almost in two minutes upon interaction with uranyl ion (Fig. 10). As seen from Fig. 10, the complex formed was decomposed almost in 4 min in the presence of dithionite.

Binding Mode of *AcI* with UO_2^{2+}

The fluorescence titration reveals that three of uranyl ions bind to the two of *AcI* molecules (Fig. 11). The molecular model of the complex $AcI_2(UO_2^{2+})_3$ as depicted in Fig. 11 indicates that urethane and the tertiary amine moieties of *AcI* can participate in the binding with uranyl ions.

Conclusions

A fluorescent receptor, isocyanatopropyl trimethoxysilane grafted 9-amino acridine for selectively sensing of uranyl ions has been synthesized and characterized. The study presents the appropriate selectivity for the determination of UO_2^{2+} ion based on fluorescence enhancement of *AcI* upon complex formation with uranyl ion. *AcI* exhibits turn-on type fluorescence phenomena towards uranyl ion in pH-acidic solution. Fluorescence emission intensity of *AcI* increased upon titration of uranyl ions and red shift of about 7 nm was observed. In order to eliminate the interference effect of mercury (II) ion on assay of uranyl ion, UV-vis titration was carried out. It was observed that peak maximum of *AcI* in UV-vis spectrum shifted to shorter wavelength region and absorbance value increased upon titration with uranyl ion. These behaviors of *AcI*, i.e. functioning in a turn-on mode, displaying high selectivity over mercury ion and other cations, and having a unique reversible function, make *AcI* a promising candidate as a fluorescent sensor for uranyl ion.

Acknowledgments We thank research project supported by Istanbul Technical University (BAP, Project No: 36236).

References

1. Bernhard G, Geipel G, Brendler V, Nitsche H (1996) Speciation of uranium in seepage waters of a mine tailing pile studied by time-resolved laser-induced fluorescence spectroscopy (TRLFS). Radiochim Acta 74:87–91
2. Bostick BC, Fendorf S, Barnett MO, Jardine PM, Brooks SC (2002) Uranyl surface complexes formed on subsurface media from DOE facilities. Soil Sci Soc Am J 66:99–108
3. deLemos JL, Bostick BC, Quicksall AN, Landis JD, George CC, Slagowski NL, Rock T, Brugge D, Lewis J, Durant JL (2008) Rapid dissolution of soluble uranyl phases in arid, mine-impacted catchments near Church Rock. Environ Sci Technol 42:3951–3957
4. Kowal-Fouchard A, Drot R, Simoni E, Ehrhardt JJ (2004) Use of spectroscopic techniques for uranium(VI)/montmorillonite interaction modeling. Environ Sci Technol 38:1399–1407
5. Chang HS, Gregory VK, Wang Z, Zachara MJ (2006) Adsorption of uranyl on gibbsite: a time-resolved laser-induced fluorescence spectroscopy study. Environ Sci Technol 40:1244–1249
6. Torgov VG, Demidova MG, Saprykin AI, Nikolaeva IV, Us TV, Chebykin EP (2002) Extraction preconcentration of uranium and thorium traces in the analysis of bottom sediments by ınductively coupled plasma mass spectrometry. J Anal Chem 57:303
7. Kandaz M, Güney O, Senkal FB (2009) Fluorescent chemosensor for Ag(I) based on amplified fluorescence quenching of a new phthalocyanine bearing derivative of benzofuran. Polyhedron 28:3110–3114
8. Güney O, Cebeci FÇ (2010) Molecularly ımprinted fluorescent polymer as a chemosensor for the detection of mercury ıons in aqueous media. J Applied Polym Sci 117:2373–2379
9. Karagöz F, Güney O, Bilgiçli AT (2012) Acridine-derivated receptor for selective mercury binding based on chelation-enhanced fluorescence effect. J Lumin 132:2736–2740
10. Arruda AF, Campiglia AD, Chauhan BPS, Boudjouk P (1999) New organosilicon polymer for the extraction and luminescence analysis of uranyl in environmental samples. Anal Chim Acta 396:263–272
11. Moulin C, Decambox P, Mauchein P, Pouyat D, Couston L (1996) Direct uranium(VI) and nitrate determinations in nuclear reprocessing by time resolved laser-induced fluorescence. Anal Chem 68:3204–3209
12. Berthoud T, Decambox P, Kirsch PB, Mauchien P, Moulin PC (1998) Time-resolved laser-ınduced fluorescence for lanthanides and actinides analysis. Anal Chem 60:1296
13. Moulin C, Decambox P, Trecani L (1996) Uranyl fluoride luminescence in acidic aqueous solutions. Anal Chim Acta 321:121
14. Shahabadi VZ, Akhond M, Tashkhourian J, Abbasitabar F (2009) Characterization of a new uranyl selective bulk optode; utilizing synergistic effect in optical sensor. Sensor Actuat B Chem 141:34–39
15. Alam LMN, Rahman N, Azmi SNH (2008) Optimized and validated spectrophotometric method for the determination of uranium(VI) via complexation with meloxicam. J Hazard Mater 155:261–268

16. Jie C, Zaijun L, Ming L (2008) Spectrophotometric determination of ultra trace uranium(VI) in seawater after extractive preconcentration with ionic liquid and dimethylphenylazo-salicylfluorone. Int J Environ Anal Chem 88:583–590
17. Madrakian T, Afkhami A, Mousavi A (2007) Spectrophotometric determination of trace amounts of uranium(VI) in water samples after mixed micelle-mediated extraction. Talanta 71:610–614
18. Nivens DA, Zhang Y, Angel SM (2002) Detection of uranyl ion via fluorescence quenching and photochemical oxidation of calcein. J Photochem Photobiol A: Chem 152:167–173
19. Das SK, Kedari CS, Tripathi SC (2010) Spectrophotometric determination of trace amount of uranium (VI) in different aqueous and organic streams of nuclear fuel processing using 2-(5-bromo-2-pyridylazo-5-diethylaminophenol). J Radioanal Nucl Chem 285: 675–681
20. Al-Kady AS (2012) Optimized and validated spectrophotometric methods for the determination of trace amounts of uranium and thorium using 4-chloro-N-(2,6-dimethylphenyl)-2-hydroxy-5-sulfamoylbenzamide. Sensor Actuat B: Chem 166:485–491
21. Wu M, Liao L, Zhao M, Lin Y, Xiao X, Nie C (2012) Separation and determination of trace uranium using a double-receptor sandwich supramolecule method based on immobilized salophen and fluorescence labeled oligonucleotide. Anal Chim Acta 729:80–84
22. Smith NA, Cerefice GS, Czerwinski KR (2013) Fluorescence and absorbance spectroscopy of the uranyl ion in nitric acid for process monitoring applications. J Radioanal Nucl Chem 295:1553–1560
23. Rozmaric M, Ivsic AG, Grahek Z (2007) Determination of uranium and thorium in complex samples using chromatographic separation, ICP-MS and spectrophotometric detection. Talanta 80:352–362
24. Benedik L, Vasile M, Spasova Y, Wätjen U (2009) Sequential determination of ^{210}Po and uranium radioisotopes in drinking water by alpha-particle spectrometry. Appl Radiat Isotopes 67:770–775
25. Shinotsuka K, Ebihara M (1997) Precise determination of rare earth elements thorium and uranium in chondritic meteorites by inductively coupled plasma mass spectrometry a comparative study with radiochemical neutron activation analysis. Anal Chim Acta 338:237–246
26. McMahon AW (1993) Application of analytical methods based on X-ray spectroscopy to the determination of radio nuclides. Sci Total Environ 130:285–295
27. Sundar U, Ramamurthy V, Buche V, Raoa DN, Sivadasan PC, Yadav RB (2007) Rapid measurements of concentrations of natural uranium in process stream samples via gamma spectrometry at an extraction facility. Talanta 73:476–482
28. Ganesh S, Khan F, Ahmed MK, Velavendan P, Pandey NK, Mudali UK, Pandey SK (2012) Determination of ultra traces amount of uranium in raffinates of Purex process by laser fluorimetry. J Radioanal Nucl Chem 292:331–334
29. Park M, Kim CH, Joo T (2013) Multifaceted ultrafast ıntramolecular charge transfer dynamics of (Dimethylamino) benzonitrile (DMABN). J Phys Chem A 117:370–377
30. Druzhinin SI, Kovalenko SA, Senyushkina TA, Demeter A, Zachariasse KA (2010) Intramolecular charge transfer with fluorazene and N-Phenylpyrrol. J Phys Chem A 114:1621–1632
31. Prabhu AAM, Sankaranarayanan RK, Venkatesh G, Rajendiran N (2012) Dual fluorescence of fast blue rr and fast violet B: effects of solvents and cyclodextrin complexation. J Phys Chem B 116:9061–9074
32. Wang J, Qian X, Cui J (2006) Detecting Hg2+ Ions with an ICT fluorescent sensor molecule: remarkable emission spectra shift and unique selectivity. J Org Chem 71:4308–4311
33. Jeong Y, Yoon J (2012) Recent progress on fluorescent chemosensors for metal ions. Inorg Chim Acta 381:2–14
34. Yan B, Zhou B, Wang QM (2007) Novel hybrid materials with covalent bonding and rare earth ions-induced enhancing luminescence of bridged 9-amino acridine. J Lumin 126:556–560
35. Forgues SF, Lavabre D (1999) Are fluorescence quantum yields so tricky to measure? A demonstration using familiar stationary products. J Chem Educ 76:1260
36. Pereira RV, Ferreira APG, Gehlen MH (2005) Excited-state intramolecular charge transfer in 9-aminoacridine derivative. J Phys Chem A 109:5978–5983
37. Xu Y, Liu Y, Qian X (2007) Novel cyanine dyes as fluorescent pH sensors: PET, ICT mechanism or resonance effect. J Photochem Photobiol A: Chem 190:1–8
38. de Silva AP, Rice TE (1999) A small supramolecular system which emulates the unidirectional, path-selective photoinduced electron transfer (PET) of the bacterial photosynthetic reaction centre (PRC). Chem Commun 2:163
39. Kumar M, Kumar N, Bhalla V, Kaur A (2013) Calix[4]arene-based fluorescent receptor for selective turn-on detection of Hg^{2+} ions. Supramol Chem 25:28–33
40. Nevado JJB, Pulgarı JAM, Laguna MAG (2000) Spectrofluorimetric study of the b-cyclodextrin:vitamin K3 complex and determination of vitamin K3. Talanta 53:951
41. Wanga Y, Shi LL, Sun HH, Shang ZB, Chao JB, Jin WJ (2013) A new acridine derivative as a highly selective fluoroionophore for Cu2+ in 100 % aqueous solution. J Lumin 139:16–21
42. Cheng T, Xu Y, Zhang S, Zhu W, Qian X, Duan L (2008) Highly sensitive and selective OFF-ON fluorescent sensor for cadmium in aqueous solution and living cell. J am Chem Soc 130:16160–16161
43. Guan X, Liu X, Su Z (2007) Synthesis and photophysical behaviors of temperature/ pH-sensitive polymeric materials. I. Vinyl monomer bearing 9-aminoacridine and polymers. Eur Polym J 43:3094–3105
44. Bhalla V, Tejpal R, Kumar M (2010) Rhodamine appended terphenyl: a reversible "off–on" fluorescent chemosensor for mercury ionsSens. Actuators B Chem 151:180–185